ADVANCED ELECTRONIC MATERIALS
www.advelectronicmat.de

The Role of Tie Chains on the Mechano-Electrical Properties of Semiconducting Polymer Films

*Kaichen Gu, Jonathan W. Onorato, Christine K. Luscombe, and Yueh-Lin Loo**

The mechano-electrical properties of poly(3-hexylthiophene) thin films are investigated as a function of their tie-chain content. Tie chains play an indispensable role in enabling strain-induced structural alignment and charge-transport enhancement in the strain direction. In the absence of sufficient tie chains, the external mechanical force cannot induce any significant polymer backbone alignment locally or crystallite reorientation at the mesoscale. These samples instead undergo brittle fracture on deformation, with cracks forming normal to the direction of strain; charge transport in this direction is hindered as a consequence. This mechanistic insight on strain alignment points to the promise of leveraging tie-chain fraction as a practical tuning knob for effecting the mechano-electrical properties in conjugated polymer systems.

1. Introduction

Uniaxial alignment of conjugated polymers along the channel direction has been shown as an effective method to improve the performance of field-effect transistors comprising them as active layers. As such, a wide array of techniques, including solution shearing,[1–3] off-center spin-coating,[4,5] directional epitaxial crystallization,[6] nanogroove-guided directional solvent evaporation[7] and slot-die coating,[8] and ionic liquid templating,[9] have been developed to obtain aligned conjugated polymer films. These devices demonstrate marked in-plane charge-transport anisotropy with the mobility measured along the strain direction higher than that perpendicular to the strain direction.[10]

Charge transport within a single well-organized crystallite is straightforward. Owing to the 1D p-orbital overlap along the conjugated polymer backbone,[11] charge transport is fastest along the polymer backbone, next fastest along the π-stacking direction and essentially absent in the direction of side-chain stacking.[12,13] Charge-transport anisotropy of an individual crystallite thus stems from the relative ability to transport charge along different crystallographic directions. Elucidating the microstructural origin of macroscopic charge-transport anisotropy in semicrystalline polymer films, on the other hand, is more challenging, given their structural heterogeneities across multiple length scales.[14] Charges need to navigate across multiple crystallites and the amorphous regions between crystallites, facilitated by the presence of tie chains that connect adjacent crystallites.[15,16] As such, pinpointing the bottleneck to macroscopic charge transport can be complicated, as it is often convoluted by intrachain and intracrystallite transport at the nanometer scale, and intercrystallite transport over micrometer and millimeter scales.[17,18]

Macroscopic charge transport in semicrystalline polymer films is likely limited by transport of charges through the amorphous regions, independent of crystallite orientation. While uniaxial strain can align polymer chains, promote polymer crystallization, and orient crystalline domains,[2,5,19] we surmise that tie chains that connect neighboring crystallites must also play an indispensable role as conjugated polymers undergo strain deformation in order for charge transport to be enhanced in the strain direction. Indeed, prior studies have implicated the role of intercrystallite tie chains in enabling cooperative alignment of neighboring crystallites, and accordingly, charge-transport enhancement in the strain direction.[19,20] Yet, there has been no independent verification of the role of tie chains on the mechano-electrical response of conjugated polymers, in large part because current experimental characterization tools are blind to the amorphous regions.[19] In this work, we seek to investigate the microstructural changes of conjugated polymer films upon strain alignment and elucidate the role of tie chains on their mechano-electrical properties, that is, how their electrical properties change upon external mechanical stimuli. For this study, model regioregular poly(3-hexylthiophene) (P3HT) thin films were used to examine the critical role tie chains play

K. Gu, Prof. Y.-L. Loo
Department of Chemical and Biological Engineering
Princeton University
Princeton, NJ 08544, USA
E-mail: lloo@princeton.edu
J. W. Onorato, Prof. C. K. Luscombe
Materials Science and Engineering Department
University of Washington
Seattle, WA 98195-2120, USA
Prof. C. K. Luscombe
Department of Chemistry
University of Washington
Seattle, WA 98195-1700, USA
Prof. C. K. Luscombe
Molecular Engineering & Sciences Institute
University of Washington
Seattle, WA 98195, USA
Prof. Y.-L. Loo
Andlinger Center for Energy and the Environment
Princeton University
Princeton, NJ 08544, USA
The ORCID identification number(s) for the author(s) of this article can be found under https://doi.org/10.1002/aelm.201901070.

DOI: 10.1002/aelm.201901070

during uniaxial alignment. We judiciously selected two P3HT samples having different molecular weights, P3HT_40 and P3HT_5; these samples were chosen based on results from our prior work,[21] which showed the former sample to have tie chains above the percolation threshold to support macroscopic charge transport and the latter sample to be sub-percolative. In applying the Huang–Brown framework that was originally developed to ascribe the structural origins of mechanical properties in polyolefins,[22] we assumed that P3HT adopts Gaussian chain statistics and tie chains form when the end-to-end distance of the polymer chains exceeds a critical distance between adjacent crystallites. While the details of these assumptions necessarily affect the absolute tie-chain fraction extracted, the relative tie-chain fraction of P3HT_40 and P3HT_5 is much less sensitive to these assumptions, and sensitivity analysis around these assumptions showed their tie-chain fractions to be consistently distinct, with P3HT_40 always percolated and P3HT_5 always sub-percolative.[21] From a combination of polarized optical absorbance spectroscopy and grazing-incidence X-ray diffraction results, we demonstrate that the presence of tie chains is critical for achieving strain-induced structural alignment, and macroscopic charge-transport improvement in the strain direction. In the absence of sufficient tie chains, the external mechanical force cannot induce any significant polymer backbone alignment or crystallite reorientation. These sub-percolative samples instead undergo brittle fracture upon strain, forming macroscopic cracks normal to the strain direction which severely impede charge transport along that direction. Our findings highlight how the mechano-electrical properties of semiconducting polymer samples can be modulated by tuning the fraction of tie chains, with polymers having tie-chain fractions above percolation exhibiting improved electrical properties upon strain.

2. Results and Discussion

We first strain-aligned P3HT_40 and P3HT_5 films on a polydimethylsiloxane (PDMS) substrate.[18,23] Plastically-deformed P3HT_40 and P3HT_5 films were then used as active layers in thin-film transistors, with which we assessed their mobilities along and normal to the strain direction. **Figure 1** summarizes the anisotropy in field-effect mobility of transistors comprising thin films of P3HT_40 and P3HT_5 as a function of strain. Here, we employed $R_\mu = \frac{\mu_\parallel}{\mu_\perp}$ to quantify charge-transport anisotropy, where the subscripts $\parallel$ and $\perp$ are used throughout the paper to denote quantities measured along and normal to the strain direction, respectively, and μ is the field-effect mobility extracted from thin-film transistor measurements. R_μ at unity corresponds to isotropic in-plane charge transport, which we see in unstrained P3HT_40 and P3HT_5 films. We find R_μ to be consistently above unity, and this quantity increases with increasing strain in P3HT_40. In good agreement with previous reports,[18,19] this observation suggests enhanced chain alignment and thus improved charge transport in the direction of strain with increasing strain. In stark contrast, we find R_μ to be consistently below unity with P3HT_5, and this quantity does not vary systematically with strain. The apparent charge-transport anisotropy in P3HT_5 is counter-intuitive; we will return to discuss this interesting observation later. Nonetheless, the drastic difference in their responses to strain between percolated P3HT_40 and sub-percolative P3HT_5 implicates the critical role of tie chains on the mechano-electrical properties of P3HT.

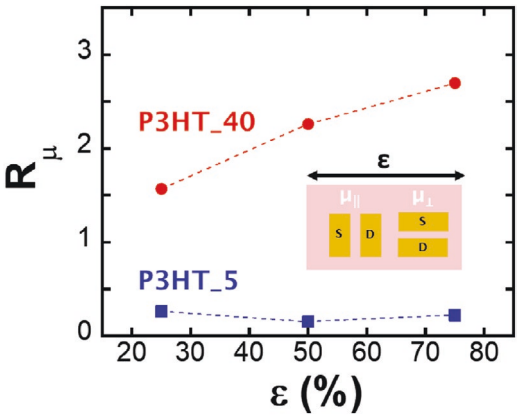

Figure 1. Anisotropy in the field-effect mobility (R_μ) of transistors comprising thin films of P3HT_40 and P3HT_5, respectively, as a function of strain. The orientations of source and drain electrodes relative to the strain direction are shown for measurements of field-effect mobilities $\mu_\parallel$ and $\mu_\perp$, respectively.

To investigate the morphological changes of the P3HT films upon strain, we first measured the polarized optical absorbance of strained films that had been transferred onto glass substrates. Because the primary optical transition dipole (π–π^*) of P3HT is oriented along its long axis, the average orientation of the polymer backbone can be estimated through these measurements.[24,25] **Figure 2** shows the normalized absorbance spectra of P3HT_40 and P3HT_5 at different strains. We find the absorbance of P3HT_40 with polarized light parallel to the strain direction ($Abs_\parallel$) to be significantly higher than that with polarized light perpendicular to the strain direction ($Abs_\perp$). This optical anisotropy can be quantified through a dichroic ratio, defined as the ratio of $Abs_\parallel$ to $Abs_\perp$. This dichroic ratio increases with increasing strain for P3HT_40, suggesting a higher extent of polymer backbone alignment. This observation is consistent with the progressively increasing R_μ with increasing strain. Interestingly, $Abs_\parallel$ and $Abs_\perp$ are very similar for P3HT_5; the negligible anisotropy in its optical absorbance with increasing strain suggests that the backbone of P3HT_5 does not align significantly with deformation. Given that the major structural difference between P3HT_40 and P3HT_5 is their tie-chain fraction, we surmise that this apparent mechano-optical response difference, like the mechano-electrical response difference observed in Figure 1, is likely to stem from differences in the extent of percolation in these two samples.

We further quantified the local order of P3HT aggregates from the vibronic features of the absorption spectra, particularly examining the absorption of the 0→0 transition near 605 nm and that of the 0→1 transition near 550 nm.[26–29] The absorption spectra of P3HT_40 and P3HT_5 thin films at different strains were fitted with the Spano model to extract the free exciton bandwidth (W) and the Gaussian line width (σ).[26,29] W varies inversely with the number of interacting thiophene mers along the polymer backbone direction and provides

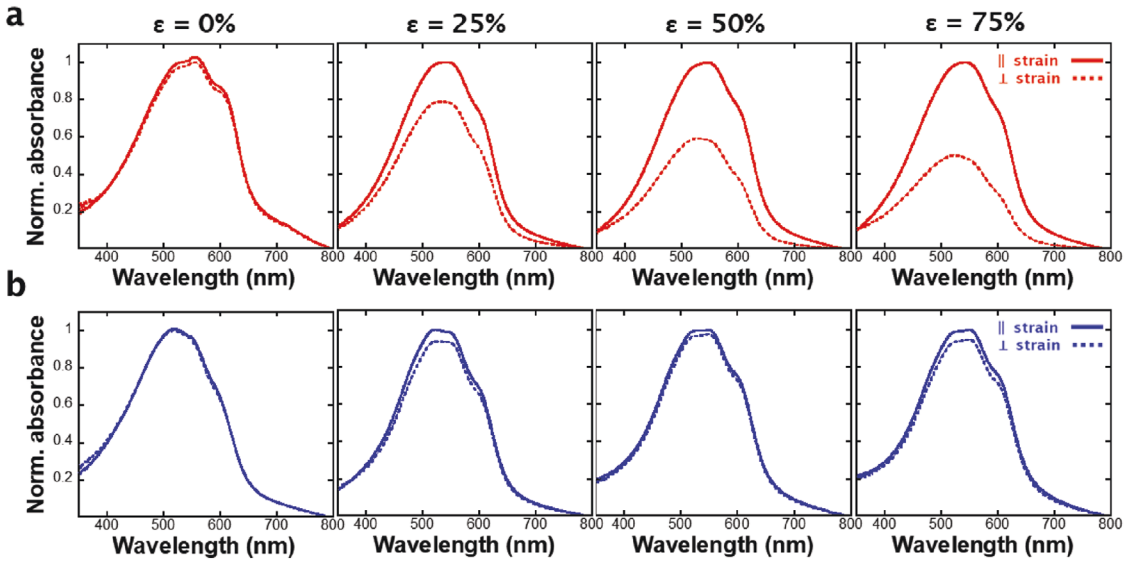

Figure 2. Normalized absorbance of a) P3HT_40 and b) P3HT_5 thin films at different strains. The absorbance spectra of the film with polarized light parallel ($Abs_{\parallel}$) and perpendicular ($Abs_{\perp}$) to the strain direction are denoted in solid and dashed lines, respectively. All absorbance curves are normalized by the maxima of $Abs_{\parallel}$.

a quantitative measure of the conjugation length and intrachain order, while σ measures the extent of interchain order. The magnitudes of W and σ are thus inversely correlated with intrachain ordering and interchain ordering, respectively.[29,30] We defined anisotropy in these quantities by: $R_W = \frac{W_{\parallel}}{W_{\perp}}$ and $R_{\sigma} = \frac{\sigma_{\parallel}}{\sigma_{\perp}}$, respectively. Figure S1, Supporting Information shows that while R_W decreases progressively below unity for P3HT_40, we find no significant anisotropy in the free exciton bandwidths for P3HT_5 with increasing strain. This comparison suggests that while the overall backbone order improves along the strain direction with increasing strain in P3HT_40, there is no marked improvement in intrachain ordering with strain in P3HT_5. Meanwhile, σ does not change significantly with increasing strain for either P3HT_40 or P3HT_5, suggesting largely invariant interchain ordering in both samples.

We performed grazing-incidence X-ray diffraction (GIXD) to investigate the crystalline structure in the P3HT thin films upon deformation. **Figure 3**a,b show 2D-GIXD images for unstrained P3HT_40 and P3HT_5 films, and those strained at 50% respectively, with the incident X-ray beam parallel (or the scattering vector nominally perpendicular) and perpendicular (or the scattering vector nominally parallel) to the strain direction. Strained or unstrained, the (100) reflection of P3HT at q = 0.39 Å^{-1} is concentrated at the meridian, confirming that crystallites in both P3HT_40 and P3HT_5 adopt a largely edge-on orientation, typical of films spin-coated from chloroform solutions of highly-regioregular P3HT on a trichlorosilane-treated substrate.[31,32] At 50% strain, the GIXD images of P3HT_40 taken with incident X-ray parallel and perpendicular to the strain direction reveal subtle deviations from that of the unstrained film, and between themselves. Indicated by white arrows in Figure 3a, we observe the development of equatorial intensity of the (100) reflection when the X-ray beam is parallel to the strain direction; this intensity is absent when the X-ray beam is perpendicular to the strain direction. We tracked these differences in the intensity distribution of the (100) reflection in P3HT_40 films through the partial pole figures in Figure 3c. In all three pole figures, the intensity is highest at low azimuthal angles (corresponding to the meridian). At high azimuthal angles approaching 90° (corresponding to the equator), the intensity of the (100) reflection of strained P3HT_40 when the X-ray beam is parallel to the strain direction is enhanced relative to the unstrained film, suggesting an increase in the fraction of crystals adopting a face-on orientation (with backbone aligned along the applied strain). In contrast, when the X-ray beam is perpendicular to the strain direction, a much weaker (100) reflection is observed at high azimuthal angles. Hence, we infer that the uniaxial strain has reoriented the crystallites in plane. The situation is very different with P3HT_5, whose GIXD images are shown in Figure 3b. The partial pole figures extracted from the GIXD images of the strained film in Figure 3d are similar in both directions, suggesting that uniaxial strain does not impart additional in-plane orientation of the crystallites in P3HT_5. This comparison suggests that tie chains play a critical role in enabling strain-induced preferential orientation of P3HT crystallites.

By quantitatively analyzing the reflections in the GIXD images, we investigated the packing of P3HT chains within crystallites. **Figure 4**a shows the out-of-plane line cuts at q_{xy} = 0 of the GIXD patterns for P3HT_40 films at different strains. We determined the characteristic spacing based on the (100) reflection, d_{100}, and estimated the corresponding crystallite correlation length, CCL, from the full width at half maximum of the reflection per Scherrer's equation.[33,34] We found that both d_{100} and CCL are largely independent of strain, as shown in Figure 4b, suggesting that while the applied strain plastically deforms the films macroscopically, it does not destroy the crystallites or the intracrystallite packing. We made comparable observations with P3HT_5, shown in Figure S2, Supporting Information.

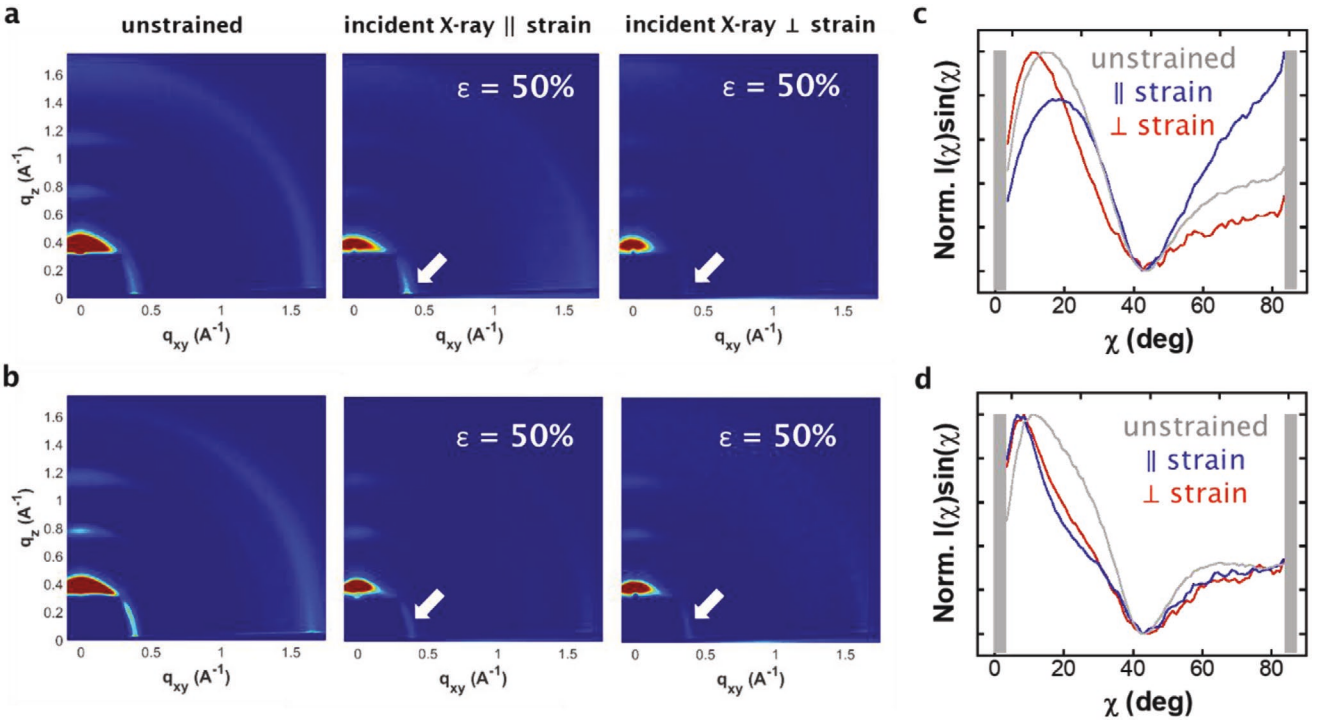

Figure 3. 2D-GIXD images for a) P3HT_40 films and b) P3HT_5 films unstrained (left panel), and at 50% strain with incident X-ray beam parallel (middle panel) and perpendicular (right panel) to strain. c–d) Pole figures constructed by tracking the normalized intensity of the (100) reflection of P3HT (q = 0.39 A^{-1}) in the GIXD images in (a) and (b), respectively, along the azimuthal angle, χ, measured from $q$xy = 0. The intensity at angle χ, I(χ), is corrected by a factor of sin(χ) to account for the thin film geometry in the GIXD. The grey-shaded areas in (c) and (d) denote the ranges of χ that are either inaccessible from GIXD measurements (low angles) or where distortions arise at the edge of the surface (high angles).

Optical micrographs in **Figure 5** show that P3HT_40 films remain intact at 75% strain, while P3HT_5 films exhibit macroscopic cracks at a comparatively small strain of 25%. In comparison, previous study has shown the crack onset strain of P3HT having M_W of 135 kg mol^{-1} to be above 120%,[35] with this quantity dependent on molecular weight.[35,36] Polymers with lower molecular weights have substantively fewer tie chains and hence crack at lower strains.[15,37] Hence, the observation that P3HT_5 exhibits brittle fracture upon strain strongly supports the lack of tie-chain connectivity to be the primary structural feature responsible. Other structural features, such as the shape anisotropy of crystallites, can also affect the mechanical response of P3HT, but changes in shape anisotropy cannot result in a brittle response.[38,39] The cracks in P3HT_5, which run perpendicular to the strain direction, severely impede charge transport along the strain direction, drastically

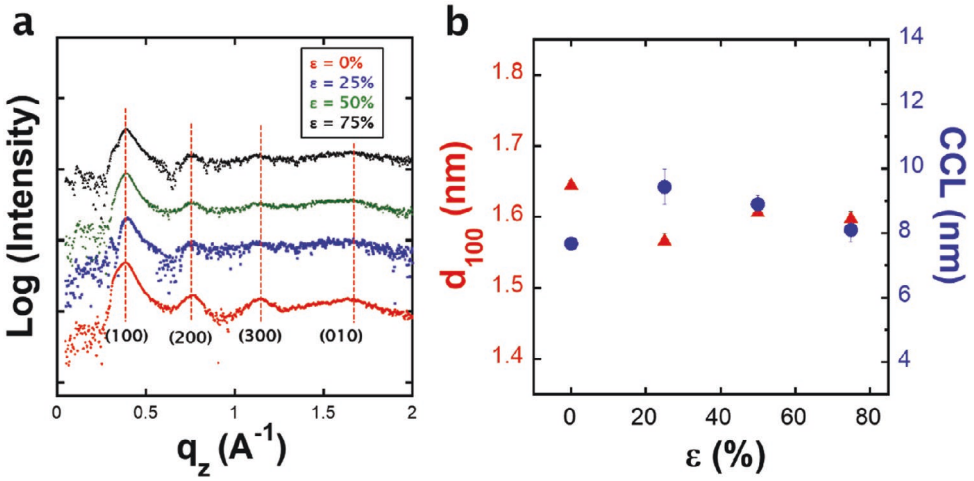

Figure 4. a) Out-of-plane line cuts at $q$xy = 0 of the GIXD profiles for P3HT_40 films at different strains. b) Characteristic spacing derived from the (100) reflection (d_{100}) and the crystallite correlation length (CCL) for P3HT_40 as a function of strain.

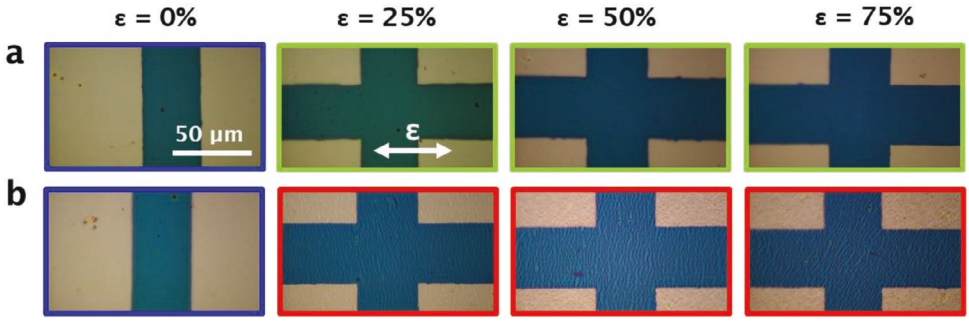

Figure 5. Optical micrographs of the active channels of transistors comprising a) P3HT_40 and b) P3HT_5, at different strains. Blue border indicates unstrained films; green border indicates strained films that are macroscopically continuous; red border indicates strained films that exhibit visible cracks. The scale bar and highlighted strain direction apply to all micrographs.

decreasing overall charge transport. Returning to Figure 1, we thus believe these cracks to be responsible for why R_μ is consistently below unity in strained P3HT_5 samples.

Combining our structural and morphological characterizations across length scales with the electrical measurements of strained P3HT_40 and P3HT_5 films, we have constructed a microscopic picture that describes the mechano-electrical response of these materials. This picture—and the difference between P3HT_40 and P3HT_5, are schematized in **Figure 6**, highlighting the critical role of polymer tie chains on the mechano-electrical properties of P3HT. Unstrained P3HT films are semicrystalline, with crystallites randomly oriented in-plane in an amorphous matrix. Straining P3HT_40 results in preferential orientation of crystallites in the direction of strain. From our experiments, we infer that the external mechanical force stretches and aligns the interconnecting tie chains along the strain direction, which causes a concomitant reorientation of crystallites and preferential alignment of polymer backbone. These morphological changes in turn lead to enhanced macroscopic charge transport along the strain direction. As we have shown, this improved macroscopic charge transport need not come from an increase in crystallinity. Rather, it can stem from

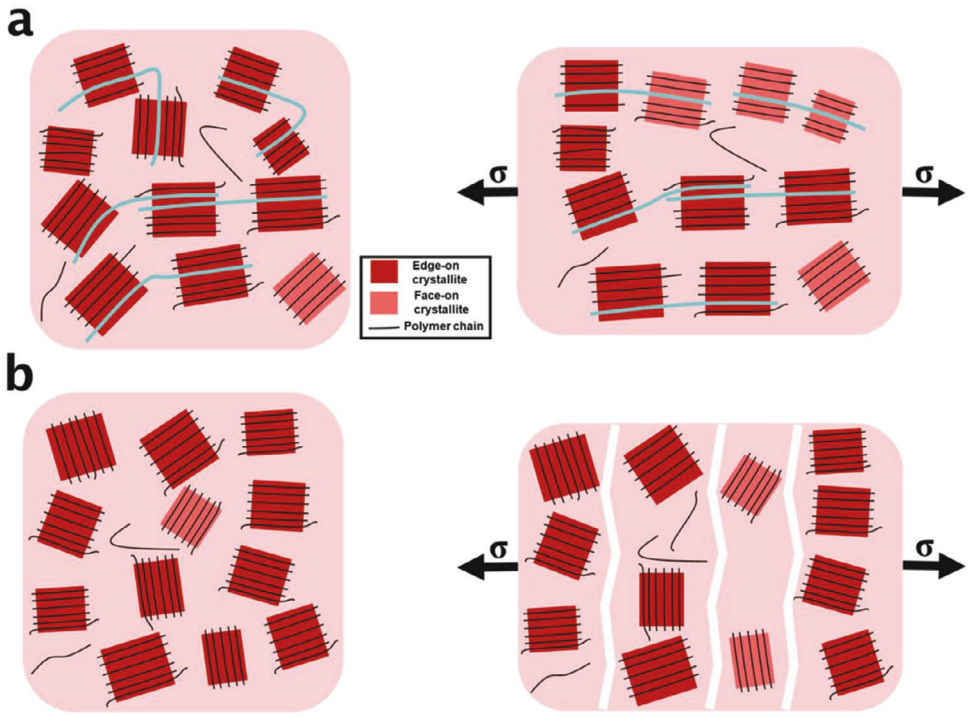

Figure 6. Schemes of unstrained and strained a) P3HT_40 and b) P3HT_5. Unstrained P3HT films are semicrystalline; the crystallites are randomly oriented in-plane. P3HT_40 has a tie-chain fraction above the percolation threshold; straining P3HT_40 thus induces the crystallites to preferentially orient along the strain direction, given their interconnectivity. P3HT_5, on the other hand, has a tie-chain fraction below the percolation threshold; the crystallites in such films are largely isolated from each other. Tie chains are highlighted in cyan in the schemes. Straining P3HT_5 does not induce any significant preferential orientation of the crystallites given the lack of connectivity. The absence of tie chains results in brittle fracture when P3HT_5 films are strained.

improved intrachain transport and a reduced number of slower interchain hopping events.[10] By the same token, we believe that tie chains are also responsible for efficient charge transport in donor-acceptor copolymers that have rigid backbones but exhibit poor long-range order.[15,40]

Interestingly, while an edge-on orientation is generally thought to be more favorable for lateral charge transport than face-on orientation,[12] our results indicate that charge transport along the strain direction can be enhanced despite a larger face-on population of crystallites induced through strain deformation in P3HT_40. This observation further highlights the importance of intercrystallite connectivity, without which isolated crystallites would less likely contribute to in-plane macroscopic charge transport.[14,18,41] Supporting this position are our results with P3HT_5, which does not possess sufficient tie chains to support percolation, and its neighboring crystallites in essence isolated from one another. In the absence of intercrystallite connectivity, straining P3HT_5 does not induce any significant reorientation of the crystallites. Consistently, the absence of tie chains also leads to brittle fracture when P3HT_5 films are strained, drastically disrupting overall charge transport. The mechano-electrical properties of P3HT_5 have not been observed in previous studies in large part because such studies have largely been carried out on samples with molecular weights sufficiently high to support percolation, which in itself implicitly assumes the significance of tie chains.[18,19,41]

We extended our analyses to P3HT_5/40, a homopolymer blend of P3HT_5 and P3HT_40, (with the mass fraction of P3HT_40, $w_{\text{higher-M}}$, of 25%). This blend sample has a corresponding intermediate tie-chain fraction between that of P3HT_5 and P3HT_40.[21] P3HT_5/40 films start to crack at strains above 25%, as shown in **Figure 7**a. Consistent with our homopolymer study above, we find R_{μ} to be above unity for uncracked films (25% strain) and below unity for cracked films (50% and 75% strain), as shown in Figure 7b. Mobilities of transistors comprising thin films of P3HT_40, P3HT_5/40 ($w_{\text{higher-M}}$ = 25%), and P3HT_5, are summarized in Figure S3, as a function of strain.

We compared the strained-induced morphological changes of the P3HT samples having different tie-chain fractions. The dichroic ratio (R_{abs}), which quantifies the anisotropy in optical absorbance and measures the extent of polymer backbone alignment, is shown in **Figure 8**a as a function of strain. The slopes of linear fits to the data presented in Figure 8a quantifies the extent of backbone alignment with strain. These slopes are plotted as a function of the P3HT tie-chain fraction, as extracted from the Huang–Brown Framework previously detailed elsewhere,[21] in Figure 8b. At any given strain, we find the extent of backbone alignment to increase monotonically with the tie-chain fraction, although a functional form for predicting the dichroic ratio from applied strain and tie-chain fraction is subject to future studies.

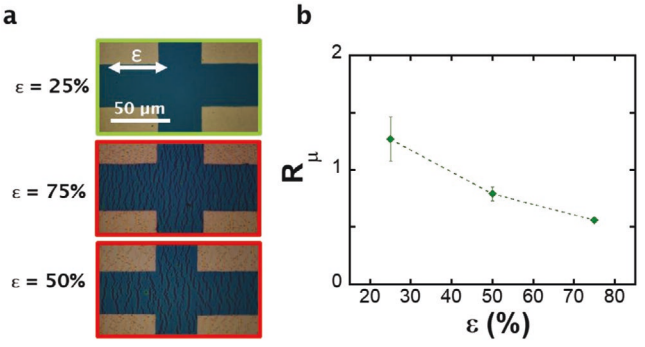

Figure 7. a) Optical micrographs of the active channels of transistors comprising P3HT_5/40 ($w_{\text{higher-M}}$ = 25%), at different strains. The scale bar and highlighted strain direction apply to all micrographs. b) Anisotropy in the field-effect mobility of transistors comprising thin films of P3HT_5/40 ($w_{\text{higher-M}}$ = 25%) as active layers as a function of strain.

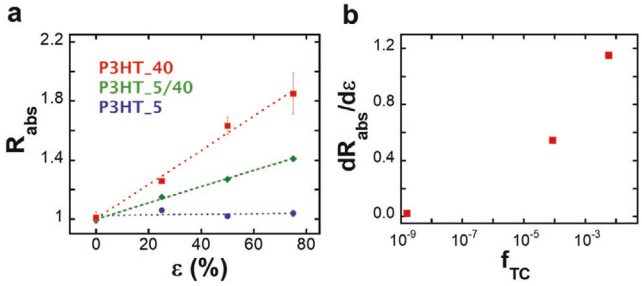

Figure 8. a) The dichroic ratio of thin films of P3HT_40, P3HT_5/40 ($w_{\text{higher-M}}$ = 25%), and P3HT_5, as a function of strain. Dashed lines represent linear fits to the data series. b) The slopes of these linear fits as a function of the tie-chain fraction, as extracted from previous work.[21]

3. Conclusion

In summary, we investigated the morphological changes in P3HT samples having known tie-chain fractions and the changes in their charge-transport properties upon strain alignment. This study reinforces the critical role of tie chains in enabling effective strain-induced structural alignment, and thus resulting in charge-transport enhancement in the direction of strain. In the absence of tie chains, the external mechanical force does not induce any significant alignment of the polymer backbone or reorientation of the crystallites in semicrystalline conjugated polymer films. By altering the tie-chain fraction of conjugated polymer samples, we can change their mechano-electrical properties, tailored to specific application needs.

4. Experimental Section

Materials: All solvents were purchased from Fisher Scientific and used as received. Hexylltrichlorosilane (HTS) was purchased from Sigma Aldrich and used as-received. P3HT was synthesized per literature procedure.[42] P3HT_40 has a number-average molecular weight (M_n) of 40 kg mol^{-1} and dispersity ($Đ$) of 1.27, and P3HT_5 has M_n of 5 kg mol^{-1} and $Đ$ of 1.26, as determined in previous study.[43] PDMS (Sylgard 184, Dow Corning) was prepared by mixing the liquid elastomer with the crosslinker at a weight ratio of 15:1 and heating for 4 h at 70 °C.

Film Preparation: P3HT was dissolved into chloroform at ≈8 mg mL^{-1}. Silicon substrates were cleaned by sonication in deionized water, acetone, isopropanol and then dried with nitrogen stream, prior to the film transfer. After cleaning, the substrates were placed in a 5 vol% solution of HTS in toluene. After 4 h at 90 °C, the substrates were removed from the solution and cleaned with toluene. The P3HT

solution was spin-coated at 1000 rpm for 45 s onto HTS-treated silicon substrates. HTS, instead of octyltrichlorosilane (OTS),[18] was used for treating the surface, owing to weak film-forming ability of P3HT_5 on OTS-treated surfaces.

Film Alignment: The P3HT film on HTS-treated silicon substrate was laminated to a dog-bone-shaped PDMS slab. The substrate was peeled off, leaving behind the complete P3HT film on the PDMS slab. The resulting P3HT–PDMS composite was then strained on a custom-made strain stage, at a strain rate of ≈0.5% s^{-1}. The composite was strained to varying extents and held in place, plastically deforming the P3HT films. These strained P3HT films were then laminated onto a secondary substrate. Effective film transfer needs to be performed through fast removal followed by slow retrieval, because of the kinetic dependence of the adhesion process between PDMS and the film.[44] The optical images of the strained films were collected post-transfer. All the secondary receiving substrates, either glass substrates or silicon wafers, were pre-cleaned following the above procedures.

Transistor Fabrication and Characterization: The P3HT film was transferred from the PDMS slab to precleaned silicon wafers, with 300 nm of thermally-grown SiO_2 (purchased from Process Specialties, Inc.) were used as gate and gate dielectric, respectively. All the thin-film transistors were fabricated in a bottom-gate-top-contact manner. 50 nm of gold was then thermally evaporated onto the substrates at a rate of ≈1.5 A s^{-1}, through a stencil mask with channel widths of 90 µm and channel lengths of 37 µm. All transistors were tested under vacuum using an Agilent 4155C semiconductor parameter analyzer. The hole mobilities were estimated in the saturation regime at a source-drain voltage of −80 V.

Optical Absorption Measurements: The P3HT film was transferred from the PDMS slab to precleaned glass substrates. Absorption spectra were recorded using an Agilent Technologies Cary 5000 spectrophotometer.

Grazing-Incidence X-Ray Diffraction: The P3HT film was transferred from the PDMS slab to precleaned silicon wafers. GIXD was performed at the G1 station at the Cornell High Energy Synchrotron Source. X-rays at 9.9 keV were selected using a beryllium single-crystal monochromator. A 0.2 × 3 (V × H) mm^2 beam was defined with motorized slits. The X-ray beam was aligned between the critical angles of the film and substrate, at 0.17° with respect to the substrate. Scattered intensity was collected using a 640-element 1D diode array. Scattered intensity was collected by a 2D CCD detector, placed 120 mm away from the sample. All presented GIXD images have been background subtracted.

Supporting Information

Supporting Information is available from the Wiley Online Library or from the author.

Acknowledgements

This work was supported by ExxonMobil through its membership in the Princeton E-filliates Partnership of the Andlinger Center for Energy and the Environment. K.G. acknowledges the Mr. and Mrs. Yan Huo *94*95 Graduate Fellowship, administered by Princeton Institute for International and Regional Studies (PIIRS). Y.-L.L. acknowledges partial funding from the National Science Foundation (NSF) through grant CMMI-1824674. The syntheses of P3HT samples were in part supported by the U.S. Department of Energy (DOE), Office of Science, Basic Energy Sciences (BES), under Award DE-SC0020046 (reagent purchase) and in part by the State of Washington through the University of Washington Clean Energy Institute and via funding from the Washington Research Foundation (partial financial support for J.W.O.). Portion of this work was conducted at the Cornell High Energy Synchrotron Source (CHESS), which is supported by NSF under award DMR-1332208. The authors would like to thank Dr. Mark M. Disko and Dr. August W. Bosse for useful discussions.

Conflict of Interest

The authors declare no conflict of interest.

Keywords

chain alignment, charge transport, conjugated polymers, field-effect transistors, organic electronics

Received: October 1, 2019
Revised: November 29, 2019
Published online:

[1] Y. Diao, B. C. K. Tee, G. Giri, J. Xu, D. H. Kim, H. A. Becerril, R. M. Stoltenberg, T. H. Lee, G. Xue, S. C. B. Mannsfeld, Z. Bao, *Nat. Mater.* **2013**, *12*, 665.
[2] Y. Diao, Y. Zhou, T. Kurosawa, L. Shaw, C. Wang, S. Park, Y. Guo, J. A. Reinspach, K. Gu, X. Gu, B. C. K. Tee, C. Pang, H. Yan, D. Zhao, M. F. Toney, S. C. B. Mannsfeld, Z. Bao, *Nat. Commun.* **2015**, *6*, 7955.
[3] J. H. Li, Y. Xi, L. D. Pozzo, J. T. Xu, C. K. Luscombe, *J. Mater. Chem. C* **2017**, *5*, 5128.
[4] Y. Yuan, G. Giri, A. L. Ayzner, A. P. Zoombelt, S. C. B. Mannsfeld, J. Chen, D. Nordlund, M. F. Toney, J. Huang, Z. Bao, *Nat. Commun.* **2014**, *5*, 1.
[5] H. Wang, L. Chen, R. Xing, J. Liu, Y. Han, *Langmuir* **2015**, *31*, 469.
[6] A. Hamidi-Sakr, D. Schiefer, S. Covindarassou, L. Biniek, M. Sommer, M. Brinkmann, *Macromolecules* **2016**, *49*, 3452.
[7] H. R. Tseng, L. Ying, B. B. Y. Hsu, L. a. Perez, C. J. Takacs, G. C. Bazan, A. J. Heeger, *Nano Lett.* **2012**, *12*, 6353.
[8] A. K. K. Kyaw, L. S. Lay, G. W. Peng, J. Changyun, Z. Jie, *Chem. Commun.* **2016**, *52*, 358.
[9] J. Soeda, H. Matsui, T. Okamoto, I. Osaka, K. Takimiya, J. Takeya, *Adv. Mater.* **2014**, *26*, 6430.
[10] D. Khim, A. Luzio, G. E. Bonacchini, G. Pace, M. J. Lee, Y. Y. Noh, M. Caironi, *Adv. Mater.* **2018**, *30*, 1705463.
[11] B. G. Kim, E. J. Jeong, J. W. Chung, S. Seo, B. Koo, J. Kim, *Nat. Mater.* **2013**, *12*, 659.
[12] H. Sirringhaus, P. J. Brown, R. H. Friend, M. M. Nielsen, K. Bechgaard, B. M. W. Langeveld-Voss, A. J. H. Spiering, R. A. J. Janssen, E. W. Meijer, P. Herwig, D. M. de Leeuw, *Nature* **1999**, *401*, 685.
[13] A. Salleo, *Mater. Today* **2007**, *10*, 38.
[14] K. Gu, Y.-L. Loo, *J. Polym. Sci., Part B: Polym. Phys.* **2019**, *57*, 1559.
[15] R. Noriega, J. Rivnay, K. Vandewal, F. P. V Koch, N. Stingelin, P. Smith, M. F. Toney, A. Salleo, *Nat. Mater.* **2013**, *12*, 1038.
[16] A. R. Chew, R. Ghosh, V. Pakhnyuk, J. Onorato, E. C. Davidson, R. A. Segalman, C. K. Luscombe, F. C. Spano, A. Salleo, *Adv. Funct. Mater.* **2018**, *28*, 1804142.
[17] L. H. Jimison, M. F. Toney, I. McCulloch, M. Heeney, A. Salleo, *Adv. Mater.* **2009**, *21*, 1568.
[18] B. O'Connor, R. J. Kline, B. R. Conrad, L. J. Richter, D. Gundlach, M. F. Toney, D. M. DeLongchamp, *Adv. Funct. Mater.* **2011**, *21*, 3697.
[19] B. T. O'Connor, O. G. Reid, X. Zhang, R. J. Kline, L. J. Richter, D. J. Gundlach, D. M. Delongchamp, M. F. Toney, N. Kopidakis, G. Rumbles, *Adv. Funct. Mater.* **2014**, *24*, 3422.

[20] D. Wu, M. Kaplan, H. W. Ro, S. Engmann, D. A. Fischer, D. M. DeLongchamp, L. J. Richter, E. Gann, L. Thomsen, C. R. McNeill, X. Zhang, *Chem. Mater.* **2018**, *30*, 1924.
[21] K. Gu, C. R. Snyder, J. Onorato, C. K. Luscombe, A. W. Bosse, Y.-L. Loo, *ACS Macro Lett.* **2018**, *7*, 1333.
[22] Y.-L. Huang, N. Brown, *J. Mater. Sci.* **1988**, *23*, 3648.
[23] M. L. Chabinyc, A. Salleo, Y. Wu, P. Liu, B. S. Ong, M. Heeney, I. McCulloch, *J. Am. Chem. Soc.* **2004**, *126*, 13928.
[24] M. C. Gurau, D. M. Delongchamp, B. M. Vogel, E. K. Lin, D. A. Fischer, S. Sambasivan, L. J. Richter, *Langmuir* **2007**, *23*, 834.
[25] D. M. Delongchamp, R. J. Kline, A. Herzing, *Energy Environ. Sci.* **2012**, *5*, 5980.
[26] F. C. Spano, *J. Chem. Phys.* **2005**, *122*, 234701.
[27] F. C. Spano, *Chem. Phys.* **2006**, *325*, 22.
[28] J. Clark, J. F. Chang, F. C. Spano, R. H. Friend, C. Silva, *Appl. Phys. Lett.* **2009**, *94*, 2007.
[29] S. T. Turner, P. Pingel, R. Steyrleuthner, E. J. W. Crossland, S. Ludwigs, D. Neher, *Adv. Funct. Mater.* **2011**, *21*, 4640.
[30] J. Gierschner, Y. Huang, B. Van Averbeke, J. Cornil, R. H. Friend, D. Beljonne, *J. Chem. Phys.* **2009**, *130*, 044105.
[31] R. Joseph Kline, M. D. McGehee, M. F. Toney, *Nat. Mater.* **2006**, *5*, 222.
[32] L. H. Jimison, S. Himmelberger, D. T. Duong, J. Rivnay, M. F. Toney, A. Salleo, *J. Polym. Sci., Part B: Polym. Phys.* **2013**, *51*, 611.
[33] Z. Bao, J. Locklin, *Organic Field-Effect Transistors*, CRC Press, Boca Raton, FL **2007**.
[34] A. Salleo, R. J. Kline, D. M. DeLongchamp, M. L. Chabinyc, *Adv. Mater.* **2010**, *22*, 3812.
[35] N. Balar, B. T. O'Connor, *Macromolecules* **2017**, *50*, 8611.
[36] D. Rodriquez, J.-H. Kim, S. E. Root, Z. Fei, P. Boufflet, M. Heeney, T.-S. Kim, D. J. Lipomi, *ACS Appl. Mater. Interfaces* **2017**, *9*, 8855.
[37] S. Himmelberger, K. Vandewal, Z. Fei, M. Heeney, A. Salleo, *Macromolecules* **2014**, *47*, 7151.
[38] N. Brown, I. M. Ward, *J. Mater. Sci.* **1983**, *18*, 1405.
[39] X. Lu, R. Qian, N. Brown, *Polymer.* **1995**, *36*, 4239.
[40] X. Zhang, H. Bronstein, A. J. Kronemeijer, J. Smith, Y. Kim, R. J. Kline, L. J. Richter, T. D. Anthopoulos, H. Sirringhaus, K. Song, M. Heeney, W. Zhang, I. McCulloch, D. M. DeLongchamp, *Nat. Commun.* **2013**, *4*, 2238.
[41] D. Gargi, R. J. Kline, D. M. DeLongchamp, D. A. Fischer, M. F. Toney, B. T. O'Connor, *J. Phys. Chem. C* **2013**, *117*, 17421.
[42] H. A. Bronstein, C. K. Luscombe, *J. Am. Chem. Soc.* **2009**, *131*, 12894.
[43] K. Gu, J. Onorato, S. S. Xiao, C. K. Luscombe, Y.-L. Loo, *Chem. Mater.* **2018**, *30*, 570.
[44] M. A. Meitl, Z. T. Zhu, V. Kumar, K. J. Lee, X. Feng, Y. Y. Huang, I. Adesida, R. G. Nuzzo, J. A. Rogers, *Nat. Mater.* **2006**, *5*, 33.

